DIGITAL CONTROL OF ARTIFICIAL SATELLITES WITH FLEXIBLE APPENDAGES

Marcelo Ricardo Alves da Costa Tredinnick
Marcelo Lopes de Oliveira e Souza / Luiz Carlos Gadelha de Souza
INPE : National Institute for Space Research / CMC : Space Mech. and Control Course / Electronics and Simulation Laboratory
Av. dos Astronautas, 1758, CEP: 12201-970, Jardim da Granja. São José dos Campos – SP – Brazil.
tredinnick@dem.inpe.br / marcelo@dem.inpe.br / gadelha@dem.inpe.br

Abstract

This work discusses and simulates the discrete-time control of artificial satellites with flexible appendages, and its stability in function of growing sampling periods. Due to mission needs the dimensions of the appendages tend to increase becoming more flexible. As a result, it is important to investigate the effects of digital characteristics such as sampling period, delays (in inputs, processing and outputs) and amplitude quantization on it. In this work only the sampling period effects are investigated. The discrete-time PD controller design is done considering aspects such as the aliasing and the hidden oscillations. It is tested with models of an harmonic oscillator and a of the CBERS1(China-Brazil Earth Resources Satellite), comparing the analog PD with discrete-time PDs obtained by standard s-z mappings (Tustin and Schneider) and by a new mapping, using the same gains for them. Root-loci, transient and steady-state responses were used to analyze their performances. These suggest partial methods of stabilization; and that the new mapping has the best performance among the mappings tested.

Introduction

As detailed in the literature[6] ,the worldwide space trend in the next century will be the production of bigger but lighter space systems. These systems will be more flexible and deformable and then will demand the control of its vibrations and forms. To meet these new requirements such controls must have increased capabilities and must solve new problems, as the one discussed below.

This work discusses and simulates the discrete control of satellites with flexible appendages using models of an harmonic oscillator and of the CBERS-1 satellite[16]. As detailed in literature[2,4,12,17], it is interesting to use digital computers and signals in control systems, because they are cheap, practical, etc., and they offer capabilities(logical, reprogramming, etc.) convenient to build and maintain the control program of a vehicle/mission.

However, this creates a fundamental problem when the vehicle is flexible: to control infinite vibration modes (as it occurs in the real case) with a digital control that intrinsically has an upper frequency limit $\omega_N=\omega_S / 2$, where ω_S is the sampling frequency as explained below.

A first problem of a digital control is its sampling in time, especially when it is controlling flexible structures. The structures oscillate with infinite modes of vibration (maximum spectral component frequency $\omega_{max} \rightarrow \infty$), but the A/D converter samples the signal with a finite frequency called sampling frequency ω_S, where $\omega_S << \omega_{max}$ [5,17]. This causes a drastic loss, distortion or mutilation of information, by the aliasing (masking) or even hiding of the frequencies in the interval $\omega_S/2 < \omega < \omega_{max}$. So, the aliasing and the hidden oscillations will occur when the known Nyquist frequency $\omega_N=\omega_S / 2$ is less than the maximum spectral component of frequency $\omega_{máx,}$, causing effects little studied in the literature [1-17].

The discretization process can be analyzed as follows: a) given the analog system of Figure 1, where D(s) and G(s) are the controller and the plant transfer functions, respectively; we want to analyze an equivalent digital control system of Figure 2 by: b) rearranging it as in Figure 3; c) a simple block manipulation as in Figure 4; d) modeling the A/D converter as in Figure 5; e) representing it as in Figure 6.

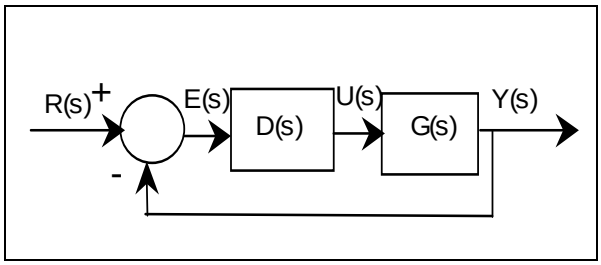

Fig. 1. Closed-loop analog control system.

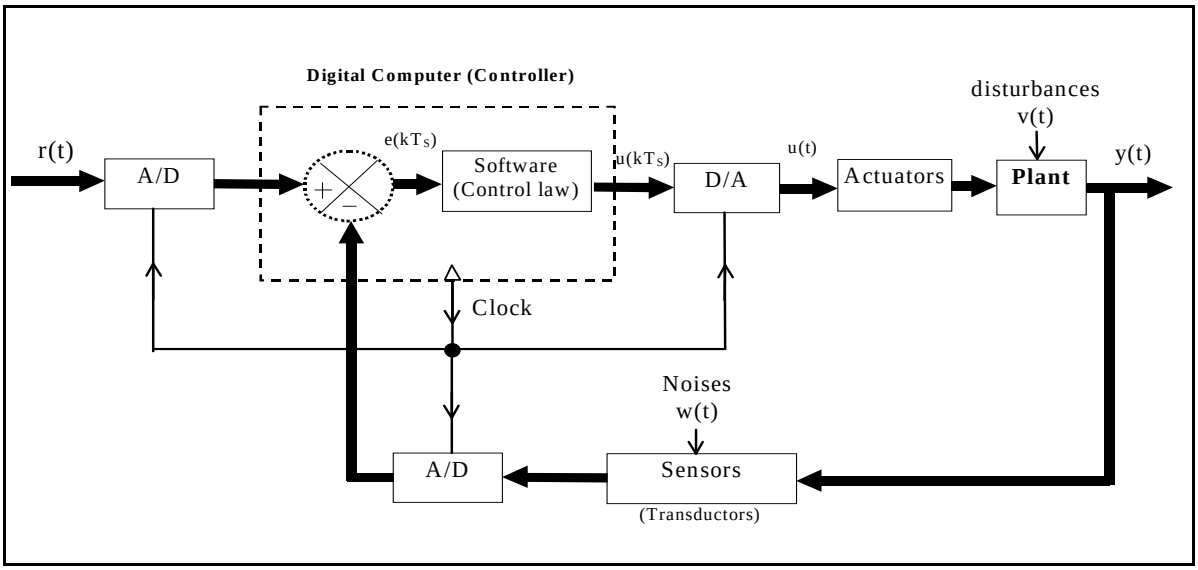

Figure 2: Closed-loop digital control system block diagram.

In Figure 6 we have the discrete-time controller D(z) and the plant Zero-Order Hold equivalent $G_{HO}(z)$ given by:

$$G_{H0}(z) = (1 - z^{-1}).Z\left\{ L^{-1}\left\{ \frac{G(s)}{s} \right\} \right\} \qquad \textbf{(1)}$$

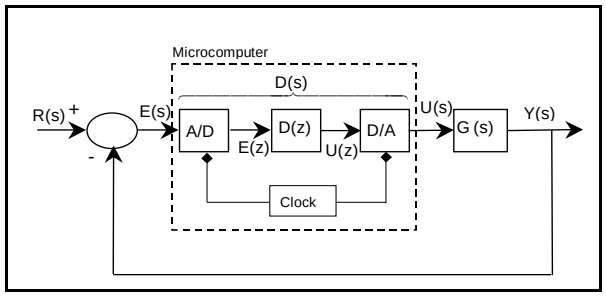

Fig.3: Closed-loop digital control system rearranged (1).

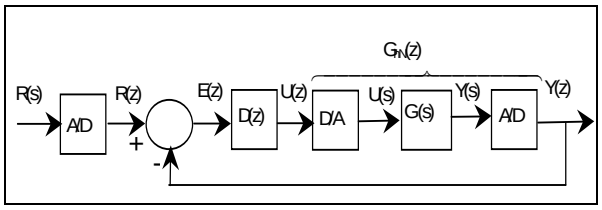

Fig.4: Closed-loop digital control system rearranged (2).

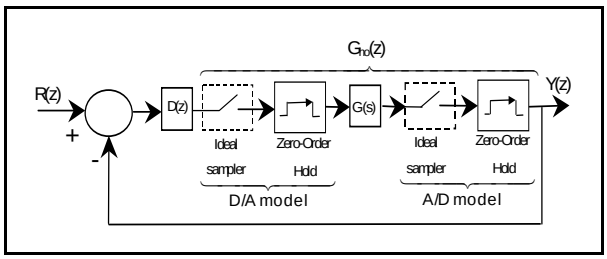

Fig.5: Closed-loop digital control system rearranged (3) with A/D and D/A sample & hold models.

In the next session we'll explain some s-z mappings.

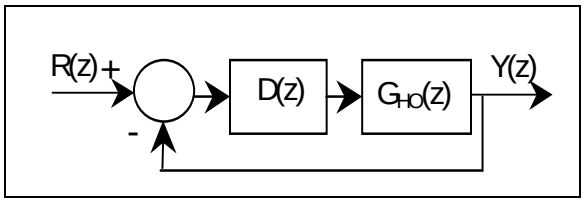

Fig.6: Discrete-time approximation to the closed-loop analog control system.

S-Z Mappings Used

All the control algorithms that are processed in a digital computer possess a structure based on finite differences equations. The standard ones used in this paper are in Table 1:

1) Backward[4,9,17] approximation: its difference equation is given by:

$$u_k = \frac{\nabla e_k}{T_S} = \frac{e_k - e_{k-1}}{T_S} \quad \textbf{(2)}$$

where T_S is the sampling period, e_k and u_k are the input and output sequences of samples when the plant is a derivative transfer function. Taking the one sided Z-transform of (2) given by the definition (3), where (f_k) is a generic sequence, we can write the s-z mapping (4).

$$F(z) \overset{\Delta}{=} Z\{f_k\} \overset{\Delta}{=} \sum_{k=0}^{+\infty} f_k . z^{-k} \quad , r_0 \le |z| \le \infty \quad \textbf{(3)}$$

$$s \sim \frac{U(z)}{E(z)} = \frac{z-1}{T_S . z} \quad \textbf{(4)}$$

2) The Forward[4,9,17] approximation has the following difference equation:

$$u_k = \frac{1}{T_s} . \nabla e_{k+1} = \frac{e_{k+1} - e_k}{T_s} \quad \textbf{(5)}$$

and, after using (3), it gives the following s-z mapping:

$$s \sim \frac{U(z)}{E(z)} = \frac{z-1}{T_s} \quad \textbf{(6)}$$

From (5) we may see its non-causality characteristic: to generate the current output u_k it is necessary to have the next input e_{k+1}! Filters designed with this kind of approximation become unstable in the closed loop system and never can be employed in real-time digital control systems.

3) The Tustin[4,9,17] (or Bilinear) approximation is better than the last two because its s-z mapping preserves stability, i.e., all the left half s-plane is mapped biunivocally in the interior of the unit circle in the z-plane, as we can see in Fig. 8. Its difference equation is given by the second-order Adams-Moulton integration formula[14]:

$$u_k = \frac{2}{T_s} . \nabla e_k - u_{k-1} \quad \textbf{(7)}$$

which, after using (3), gives the s-z mapping:

$$s \sim \frac{U(z)}{E(z)} = \frac{2}{T_s} . \frac{z-1}{z+1} \quad \textbf{(8)}$$

4) The Schneider rule[13,14,17] is described as an s-z mapping using the third-order Adams-Moulton integration formula:

$$e_k = e_{k-1} + \frac{T_S}{12} . (5.u_k + 8.u_{k-1} - u_{k-2}) \quad \textbf{(9)}$$

that can be written as follows:

$$u_k = \frac{1}{5} . \left(\frac{12}{T_S} . \nabla e_k - 8.u_{k-1} + u_{k-2} \right) \quad \textbf{(10)}$$

Applying (3) in (9) (or (10)) we have the following s-z mapping:

$$s \sim \frac{U(z)}{E(z)} = \frac{12}{T_S} . \frac{z.(z-1)}{5.z^2 + 8.z - 1} \quad \textbf{(11)}$$

As shown in Fig. 7, the Schneider s-z mapping can unstabilize the closed-loop control system when a derivative control action is employed.

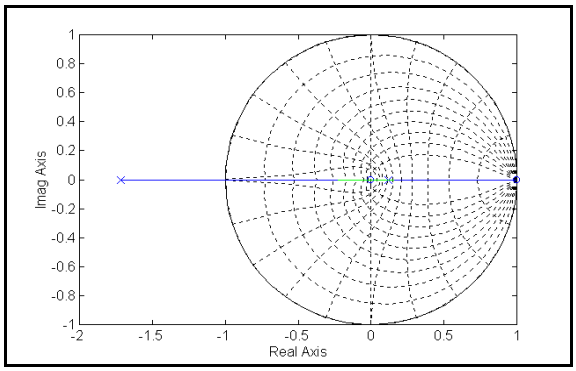

Figure 7: Unstable pole of Schneider s-z mapping.

5) The new-rule[17] has the following difference equation:

$$u_k = \frac{2}{T_s} . \nabla e_k - \xi . u_{k-1} \ , \qquad 0 < \xi < 1 \quad \textbf{(12)}$$

where ξ is a constant. The new rule was inspired in the Tustin rule displacing its $z_1 = -1$ pole to $z_1' = -\xi$, $0 < \xi < 1$. It produces good results in comparison with the classical mappings. The new rule moves the z_1' pole to the interior of the unit circle, using ξ as a design parameter.

Using (3) in (12) gives the s-z mapping:

$$s \sim \frac{U(z)}{E(z)} = \frac{2}{T_s} . \frac{z-1}{z+\xi} \quad \textbf{(13)}$$

The used discrete-time approximations can be found in Table 1. In Table 2 we can find the PD controllers designed with these approximations, where k_p and k_d are the proportional and derivative control gains.

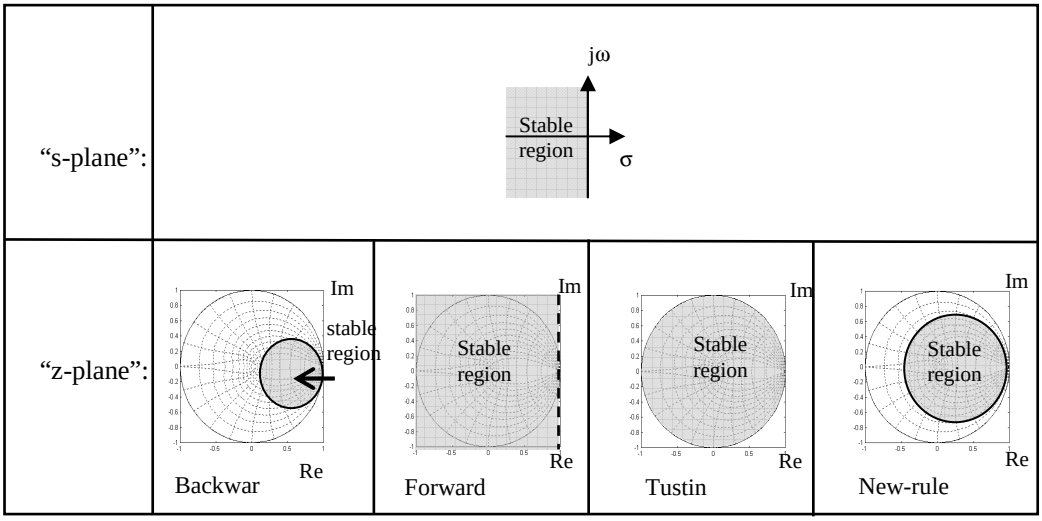

Figure 8: S-plan to z-plan mappings of the asymptotically stable region

Table 1: Discrete-time mappings

Analog case	Discrete-time mappings				
	Forward	Backward	Tustin	Schneider	New-rule
s	$\frac{z-1}{T_s}$	$\frac{z-1}{T_S.z}$	$\frac{2}{T_s}.\frac{z-1}{z+1}$	$\frac{12}{T_S}.\frac{z.(z-1)}{5.z^2+8.z-1}$	$\frac{2}{T_s}.\frac{z-1}{z+\xi}$

Table 2: D(z) discrete-time PD controllers

Analog Case of a PD controller	Discrete-time PD controllers				
	Forward	Backward	Tustin	Schneider	New-rule
$k_p + k_d.s$	$\frac{k_d}{T_S}.\left[z+\left(\frac{k_p}{k_d}.T_S-1\right)\right]$	$\left(k_p+\frac{k_d}{T_S}\right).\frac{z-\frac{k_d}{k_p.T_S+k_d}}{z}$	$\left(k_p+\frac{2k_d}{T_S}\right).\frac{z+\left(\frac{k_p.T_S-2k_d}{k_p.T_S+2k_d}\right)}{z+1}$	$\frac{\left[5k_p+\frac{12k_d}{T_S}\right]z^2+\left[8k_p-\frac{12k_d}{T_S}\right]z-k_p}{5z^2+8z-1}$	$\left(k_p+\frac{2k_d}{T_S}\right).\frac{z+\left(\frac{k_p.T_S.\xi-2k_d}{k_p.T_S+2k_d}\right)}{z+\xi}$

Table 3: Harmonic oscillator zero order hold equivalences.

		$G_{H0}(z)$
Case:	Free:	$[1-\cos(\omega_n.T_S)].\frac{z+1}{z^2-(2.\cos(\omega_n.T_S)).z+1}$
	Damped:	$\frac{z+1-2.e^{-\zeta.\omega_n.T_S}.\cos(\omega_n.T_S).z+e^{-2\zeta.\omega_n.T_S}}{\left(\cos(\omega_d.T_S)-\frac{\zeta}{\sqrt{1-\zeta^2}}.\sin(\omega_d.T_S)\right).z+e^{-2\zeta.\omega_n.T_S}+\left(\frac{\zeta}{\sqrt{1-\zeta^2}}.\sin(\omega_d.T_S)-\cos(\omega_d.T_S)\right).e^{-\zeta.\omega_n.T_S}.z}$

Plants Used

1) Free and Damped Harmonic Oscillators, whose transfer functions are:

$$G(s) = \frac{{\omega_n}^2}{s^2 + {\omega_n}^2} \quad \textbf{(15)}$$

$$G(s) = \frac{{\omega_n}^2}{s^2 + 2.\zeta.\omega_n.s + {\omega_n}^2} \quad \textbf{(16)}$$

Their discrete-time equivalents $G_{H0}(z)$, given by (1), are showed in Table 3.

2) A CBERS1 model: according to current literature[16], it employs the right-eigenvalues matrix $\Phi = [\underline{\phi}_1 \vdots \underline{\phi}_2 \vdots \underline{\phi}_3 \vdots \ldots \vdots \underline{\phi}_n]$ as the transformation matrix from a modal coordinate $\eta(t)$ to physical coordinates $X(t)$ given by:

$$\underline{X}(t) = \Phi.\underline{\eta}(t) \quad \textbf{(17)}$$

The modal equation of motion of a satellite, including the structural damping used is:

$$I.\ddot{\underline{\eta}} + 2.\zeta.diag(0,0,0,\omega_1,\omega_2,\ldots,\omega_{n-1}).\dot{\underline{\eta}} + - diag\left(0,0,0,{\omega_1}^2,{\omega_2}^2,\ldots,{\omega_{n-1}}^2\right)\underline{\eta} = \Phi^T.b_c.\underline{u} \quad \textbf{(18)}$$

where ζ is the damping ratio, I is the inertia tensor, ω_i is the natural undamped frequency, b_c is the control influence matrix and u is the control vector.
Finally, the linear differential state space equation is given by:

$$\dot{\underline{X}}(t) = A.\underline{X}(t) + B.\underline{u} \quad \textbf{(19)}$$

where:

$$\underline{X} = \begin{pmatrix} \underline{\eta} \\ \dot{\underline{\eta}} \end{pmatrix} \quad \textbf{(20)}$$

Where A and B are the matrices responsible for the system dynamics and the actuators positioning in the state space form, respectively.

Simulations

1) Harmonic-oscillator: Figures 9 and 10 show simulations of the over-damped harmonic oscillator with a PD controller designed by Tustin rule and by the new rule, i.e., using the third and fifth expressions from left to right of Table 2 as D(z), and the damped expression of Table 3 as $G_{H0}(z)$. We may see that this one stabilizes the system but the other not. Their root-loci are in Figure 11 and 12. The Forward and Schneider mappings of the PD control didn't behave well and will not be shown.

2) A model of the CBERS1 satellite: Figures 13 to 20 show the results for the Tustin mapping and for the new-rule mapping controlling the 2 modes model. We may note a strong control signal in Fig. 16 provoked probably by the sampler keying. These Figures shown very clearly that the new-rule mapping has a better performance that the Tustin mapping (note the unstable Yaw axis in Figures 13 and 16).

Conclusions

First, it is important to call the attention for the existence of the problem of instability that can be introduced in the discrete-time control systems mainly for high sampling periods T_S. The choice of the sampling period T_S , aliasing filter, control gains, structural damping, and the type of s-z mapping to design such controller in discrete time will be decisive factors for reaching stability.

Second, the new rule represents a promising alternative for the stabilization of a control system in time-discrete when the plant is a flexible structure and has high values of the sampling period T_S. The simulations with the new rule shown a better performance for the damped harmonic oscillator as for the CBERS1 model used. However, it is very important to note that this model[16] is a linear model with five modes of vibration and it does not represents all nuances of the real structure; in particular, the increasing damping with the mode number and other energy dissipative phenomena. Therefore, these conclusions are valid for the models used in this work but not necessarily for the real satellite. It is suggested to verify them with better models and/or experimentally in future works.

References

[1]Bose, N. K. Comments on S-plane to Z-plane Mapping Using a Simultaneous Equation Algorithm Based on the Bilinear Transformation. *IEEE Transactions on Automatic Control*. v.33, n.11, pp.1085-1086, Nov. 1988.

[2]Deets, D.A.; Szalai, K.J. Design and Flight Experience with a Digital Fly-by-Wire Control System Using Apollo Guidance System Hardware on an F-8 Aircraft. Stanford, California: NASA Flight Research Center, 1972. 12p. (*AIAA* paper 72-881).

[3]Diduch, C.P.; Doraiswami, R. Sample Period Effects in Optimally Designed Digital Control Systems. *Journal of Guidance, Control, and Dynamics*, v. AC-32, n.9, p.838-841, Set. 1987.

[4]Franklin, G.F.; Powell, D. *Digital Control of Dynamic Systems*. California, EUA: Addison-Wesley Publishing Company, 1981. 335p.

[5]Ginter, S.D. *Attitude Control of Large Flexible Spacecraft*. Boston, EUA. Master Thesis. MIT – Massachusetts Institute of Technology, 1978.

[6]Huntress, W.T. Nasa's Space Science Program: our Outlook for the New Millenium. *AAS* – Strengthening Cooperation in the 21st Century. AAS: San Diego, 1996. Proceedings. USA: San Diego, 1996; p.3-30.

[8]Junkins, J.L.; Kim, Y. *Introduction to Dynamics and Control of Flexible Structures*. Washington, DC: AIAA Educational Series, 1993. 444p.

[9]Katz, P. *Digital Control Using Microprocessors*. EUA: Prentice-Hall Inc., 1981. p. 293.

[10]Katz, P.; Powell, J.D. Sample Rate Selection for Aircraft Digital Control**.** *AIAA Journal*, v.13, n.8, Aug. 1975, p.975-979.

[11]Krishna, H. Computational Aspects of the Bilinear Transformation Based Algorithm for s-plane to z-plane Mapping. *IEEE Transactions on Automatic Control*. v.33, n.11, pp.1086-1087, Nov. 1988.

[12]Ohkami, Y.; Okamoto, O. & Kida; T. Simulation of a Digital Controller for Flexible Spacecraft Attitude Control. In: *2th Symposium of Dynamics and Control of Large Flexible Spacecrafts*, Blacksburg, Va. 1979. Proceed. Virginia Polytech State Un.: 1979. p. 177-192.

[13]Schneider, A.M.; Anuskiewicz, J.A.; Barghouti, I.S. Accuracy and Stability of Discrete-Time Filters Generated by High-Order s-to-z Mapping Functions. *IEEE Transactions on Automatic Control*. v.39, n.2, p.435-441, Feb. 1994.

[14]Schneider, A. M.; Kaneshige, J. T.; Groutage, F. D. Higher Order s-to-z Mapping Functions and their Applications in Digitizing Continuous-Time Filters. *Proceedings of the IEEE*. V.79; no. 11; pp. 1661-1674; Nov. 1991.

[15]Schneider, A. M.; Groutage, F. D.; Volfson, L. B. S-Plane to Z-Plane Mapping Using a Simultaneous Equation Algorithm Based on the Bilinear Transformation. *IEEE Transactions on Automatic Control*. V.AC-32; no. 7; pp. 635-637; July 1987.

[16]Silva, A.R. *Estudo de Controle de um Satélite Artificial durante a Transferência Orbital e Apontamento*. (INPE-6397-TDI/613). Master Thesis – INPE, 1997. São José dos Campos, SP, Brazil. 108 p.

[17]Tredinnick, M.R.A.C. *Controle Digital de Satélites Artificiais com Apêndices Flexíveis*. Master Thesis - INPE, 1999. São José dos Campos, SP, Brazil. 212 p.

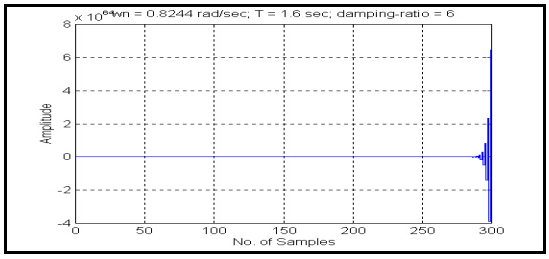

Fig. 9. Overdamped harmonic oscillator controlled by a PD designed by the Tustin- rule (T_S = 1,6 seconds): unstable.

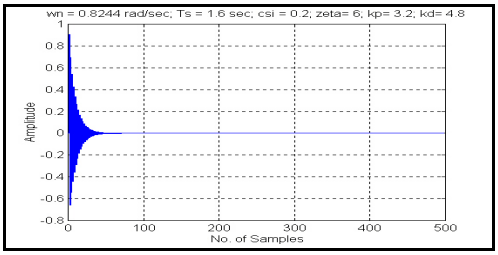

Fig. 10. Overdamped harmonic oscillator controlled by a PD designed by the new-rule (T_S = 1,6 seconds): assymptot.stable.

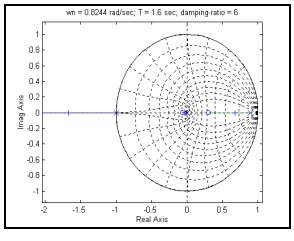

Fig. 11. Root-locus relative to Fig. 9.

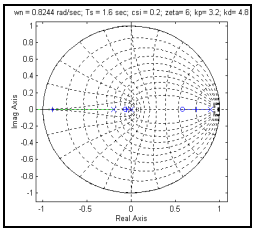

Fig. 12. Root-locus relative to Fig. 10.

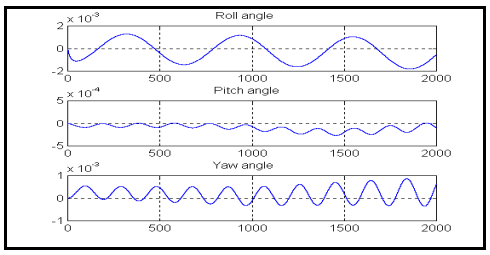

Fig. 13. Attitude angles of a CBERS1 simulation with the Tustin-rule.

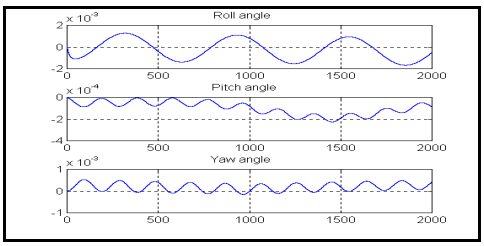

Fig. 17. Attitude angles of a CBERS1 simulation with the new-rule.

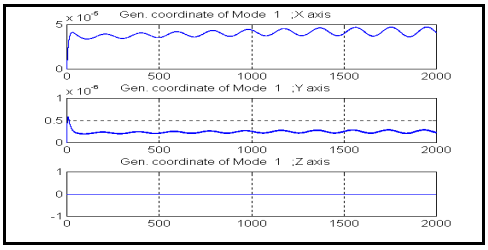

Fig. 14. Mode 1 for the simulation with the Tustin rule.

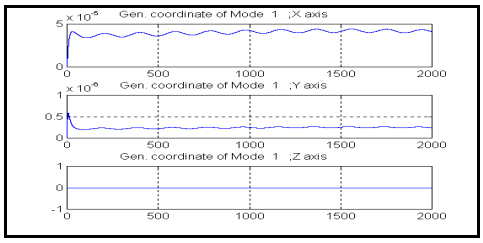

Fig. 18. Mode 1 for the simulation with the new rule.

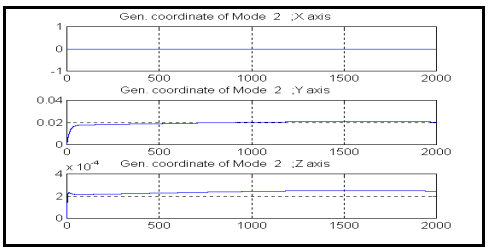

Fig. 15. Mode 2 for the simulation with the Tustin rule.

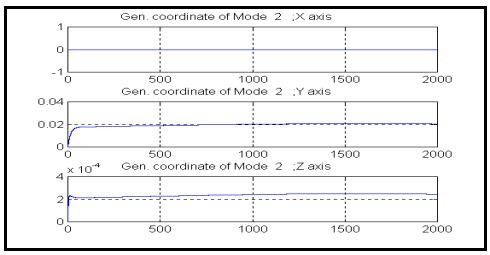

Fig. 19. Mode 2 for the simulation with the new rule.

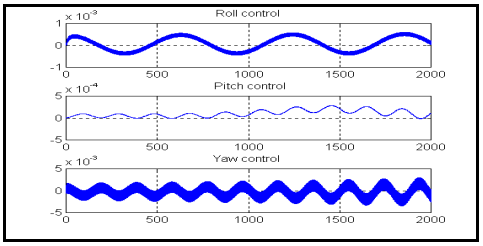

Fig. 16. PD Control signals for the CBERS1 simulation with the Tustin-rule.

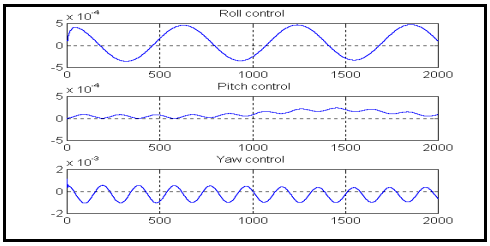

Fig. 20. PD Control signals for the CBERS1 simulation with the new-rule.